Minimum energy path and atomistic mechanism of the elementary step in oxygen diffusion in silicon: A density-functional study

Jan Felix Binder and Alfredo Pasquarello

Chaire de Simulation à l'Echelle Atomique (CSEA), Ecole Polytechnique Fédérale de Lausanne (EPFL), CH-1015 Lausanne, Switzerland

(Received 21 March 2013; revised manuscript received 2 June 2014; published 17 June 2014)

Using a density-functional scheme, we study the migration of a single O atom in a (110) plane between two adjacent bond-center sites in bulk Si. The minimum energy migration path is found through the nudged elastic band method within a generalized gradient approximation for the electronic structure. The energy barrier is then also evaluated within a hybrid functional scheme. We achieve for the transition barrier a best estimate of 2.3 eV in the generalized gradient approximation and of 2.7 eV in the hybrid functional scheme, both in fair agreement with the commonly accepted experimental value of 2.53 eV. The transition is characterized by a saddle point which does not occur at the midpoint between the two bond-center sites and by a pattern of displacements extending up to the second nearest-neighbor Si atoms. The atomistic mechanism of oxygen migration is analyzed from three complementary viewpoints involving the evolution of the structure, the Wannier centers, and the single-particle energies and wave functions. The diffusion process can be separated into two distinct parts. In one part, the exchange of the Si atoms in the first-neighbor shell of the diffusing O atom occurs through the formation of a threefold coordinated O center and an overcoordinated Si atom. In the other part, the Si–Si bond flips its position through the creation of occupied and unoccupied Si dangling bonds which give rise to states in the band gap.

DOI: 10.1103/PhysRevB.89.245306 PACS number(s): 66.30.Lw, 31.15.A−, 61.72.Yx, 82.20.Db

I. INTRODUCTION

During the last five decades, the semiconductor industry has heavily relied on the use of silicon and its native oxide as the main material constituents of electronic devices. The interface between silicon and its oxide has long been achieved by thermal oxidation, and its formation involving the interaction of oxygen with silicon has become one of the most studied atomistic processes [1–9]. According to our present understanding, oxygen diffuses in its molecular form through the oxide until the molecule dissociates by reacting with Si–Si bonds located in the interface region [1,2,6–8]. Atomistic simulations suggest that further oxygen migration across the disordered substoichiometric oxide occurs in the form of isolated interstitial atoms going through metastable transient structures in which the oxygen atoms are threefold coordinated with Si atoms [3,10]. The migration of the interstitial O atom in bulk silicon can be seen as the ultimate part of the silicon oxidation process and has thus attracted a great deal of attention. Several reviews on oxygen centers in silicon are available [11–14].

Infrared absorption experiments provided strong support that isolated oxygen atoms dissolved in silicon occupy interstitial positions between two regular nearest-neighbor atoms of the silicon lattice [15]. This model is also consistent with lattice constant and density studies [16]. The application of stress and the observation of dichroism finally confirmed the model in detail [17]. From the study of the recovery kinetics, it was additionally possible to measure the single jump diffusion process in which oxygen hops from one Si–Si bond to another. Combined with previous internal friction studies [18], this provided the first accurate measurement of the oxygen diffusion constant with an energy barrier of 2.56 eV [17]. Since that time, several experiments including long-range mass transport, internal friction, and extended stress-induced dichroism recovery studies have been performed, closely confirming the early result [19]. All the obtained data are consistent with a global fit giving an energy barrier of 2.53 eV [13,19,20]. This global agreement demonstrates in particular that the long-range diffusion results from a combination of single jumps of oxygen between neighboring Si–Si bonds of the lattice. The establishment that the diffusion proceeds through a single well-defined process is further supported by the wide temperature range extending from 350 to 1325 °C, over which the measured diffusion coefficients show a single-barrier Arrhenius behavior [13,19,20].

Several theoretical studies have attempted to model this elementary diffusion process [14,21–26]. In all theoretical studies, an isolated interstitial O atom is assumed to jump from a bond-center site to an adjacent one along a path in a (110) plane. However, the energy barriers and the diffusion path differ considerably among the various descriptions. Early density-functional-theory calculations in the local density approximation considered symmetric diffusion paths and found energy barriers in the range 1.8–2.0 eV [21,22], significantly underestimating the experimental value of 2.53 eV [13,19,20]. Using empirical potentials, Jiang and Brown pointed out that the O atom at the saddle point was not found at the midpoint of the two bond centers, and gave an overall description of the diffusion coefficient as a function of temperature in very good agreement with experiment [23]. Ramamoorthy and Pantelides recognized that the energy variations of the O diffusion process involved a complex hypersurface in a multidimensional space and argued that a barrier of ∼2.5 eV resulted from the consideration of a variety of transition paths [24]. Using a scheme based on gradient-corrected functionals, Coutinho *et al.* considered the symmetric transition state and gave an estimate of 2.2 eV for the energy barrier [14]. Through the use of gradient-corrected and hybrid functionals, Deák *et al.* then found a symmetric diffusion path with energy barriers of 2.37 and 2.69 eV, respectively [25]. More recently, Estreicher *et al.* applied the nudged-elastic-band method and compared the local density approximation to various gradient-corrected

 ©2014 American Physical Society

density functionals. These results also yielded a symmetric diffusion path with energy barriers in the range 1.78–2.01 eV [26]. These results indicate the persistence of a confusing situation with significant uncertainties regarding the diffusion path and the energy barrier. Furthermore, none of the previous theoretical works has focused on the atomistic mechanisms operative during this oxygen migration process.

In this work, we study the oxygen migration process in bulk silicon using the nudged elastic band method [27] within a density-functional-theory scheme. The minimum energy path is obtained within a generalized gradient approximation, but hybrid functionals are also used for determining the energetic profile of the transition. Our results give an asymmetric transition pathway and our estimates for the transition energy lie within 0.2 eV from the experimental value. We then address the atomistic mechanism both from the structural and electronic point of view. The electronic structure is analyzed in terms of the evolution of both maximally localized Wannier-function centers and single-particle states.

This paper is organized as follows. Section II is devoted to the determination of the minimum energy path. We first present our nudged elastic band calculations yielding an asymmetric transition state. We then compare the achieved transition state with the Y-lid configuration involving a threefold coordinated oxygen atom, which has often been identified as transition state in previous density functional calculations. We conclude this section by studying the convergence with cell size and with the number of images used in the nudged elastic band method. In Sec. III, we describe the mechanism underlying the diffusion process through the evolution of bond distances, maximally localized Wannier functions, and single-particle states. We draw conclusions in Sec. IV.

II. TRANSITION ENERGY PROFILE

A. Minimum energy path

Our electronic-structure calculations are carried out within a density-functional-theory scheme. In the nudged elastic band (NEB) [27] calculations used for determining the transition path, we use the generalized gradient approximation proposed by Perdew, Burke, and Ernzerhof (PBE) [28]. This semilocal functional combines a good accuracy for structural investigations with the computational efficiency required for a careful study of the transition path. However, the PBE leads to severe band-gap underestimations and might affect the transition energy [25]. To overcome this limitation of the PBE, we further evaluate the energy of the obtained structural configurations with the hybrid functional proposed by Heyd, Scuseria, and Ernzerhof (HSE) [29]. Since the diffusivity of O in silicon does not depend on doping [13,20], we infer that charging effects are not relevant in the diffusion process and assume the neutral charge state in our calculations.

The electron wave functions are expanded in a plane-wave basis set, and core-valence interactions are described through normconserving pseudopotentials [30]. The energy cutoff of the wave functions is set at 70 Ry. Using the PBE functional, this pseudopotential scheme yields for silicon a lattice constant of 5.46 Å and a bulk modulus of 89.2 GPa, to be compared with the experimental values of 5.43 Å [31] and 97.8 GPa [32], respectively. For α-quartz modeled with a c/a ratio fixed to its experimental value ($c/a = 1.10$ [33]), we obtain a lattice constant $a = 5.01$ Å and a bulk modulus of 34.3 GPa, in good agreement with respective experimental values of 4.86 Å [33] and 38.8 GPa [34]. For its internal structure, we find a Si–O bond of 1.62 Å and a Si–O–Si bond angle of 148°, to be compared with experimental values of 1.60 Å and 143.7° [35]. These results for silicon and α-quartz attest the quality of our pseudopotential description.

In our NEB calculations, we model bulk Si with a 64-atom cubic supercell with a side of 10.9 Å, corresponding to the equilibrium PBE lattice constant. The Brillouin zone is sampled at the Γ point. In the hybrid functional calculations, the exchange potential is treated as described in Ref. [36]. We use the QUANTUM-ESPRESSO package [37] with the implementation of the HSE functional detailed in Ref. [38]. With the 64-atom setup and the Γ-point sampling, we obtain for Si a fundamental band gap of 0.73 eV with the PBE functional and of 1.31 eV with the HSE functional, to be compared with the respective values of 0.61 and 1.20 eV, obtained upon convergence with the density of **k** points in the Brillouin zone. These values are in overall fair agreement with the respective values of 0.71 and 1.29 eV in the literature [39].

We focus on the diffusion step involving a jump of an interstitial O atom bonded to two nearest-neighbor Si atoms to a similar adjacent site in a (110) plane of the Si crystal [14]. In its equilibrium position, the interstitial O atom is situated off the Si–Si axis forming Si–O bond lengths of 1.62 Å and a Si–O–Si bond angle of 165° (cf. Fig. 1). To allow for long-range diffusion, the O atom needs to reorient around the Si–Si axis between one jump and the next. However, this reorientation plays a negligible role in the energetics of the long-range diffusion, as discussed in detail in Ref. [14]. Through specific calculations devoted to this point, we found a barrier smaller than 10 meV between symmetrically equivalent sites in which the O atom is off the Si–Si axis. To describe the transition to an adjacent site, we thus confine the path within a (110) plane and use the angle Θ_{O} which characterizes the position of the O atom with respect to the [001] direction. As illustrated in Fig. 1, this angle is centered at the unperturbed bulk position of the central Si atom taken as fixed origin. Similarly, we define the angle Θ_{Si} for $\mathrm{Si_c}$ (Fig. 1).

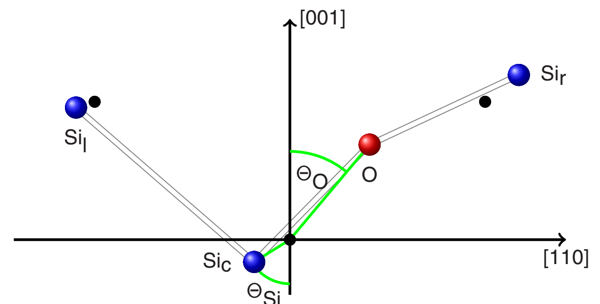

FIG. 1. (Color online) Definition of the notation used in this work for the involved Si atoms ($\mathrm{Si_l}$, $\mathrm{Si_c}$, $\mathrm{Si_r}$) and for the angles Θ_{O} and Θ_{Si} describing the evolution along the diffusion path. All atoms ($\mathrm{Si_l}$, $\mathrm{Si_c}$, $\mathrm{Si_r}$, O) are in a (110) plane of the Si crystal. The filled black disks indicate the positions of the Si atoms in an unperturbed crystal.

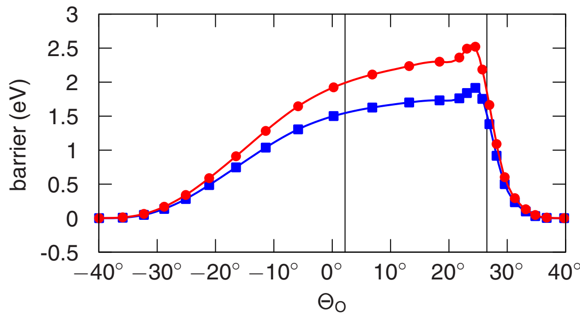

FIG. 2. (Color online) Energy of an interstitial O atom in bulk Si as a function of the angle Θ_O when jumping between two bond-center configurations (cf. Fig. 1 for the definition of Θ_O). The present minimum energy path is obtained from a NEB calculation with 25 images in a 64-atom supercell with the electronic structure described in the PBE approximation and sampled at the Γ point (squares). The calculated transition barrier is 1.91 eV. The energy evaluated at the HSE level (disks) gives a transition barrier of 2.52 eV. The symbols give the energies of the images used in the NEB calculation. The vertical lines correspond to specific structural configurations and are defined in the caption of Fig. 6.

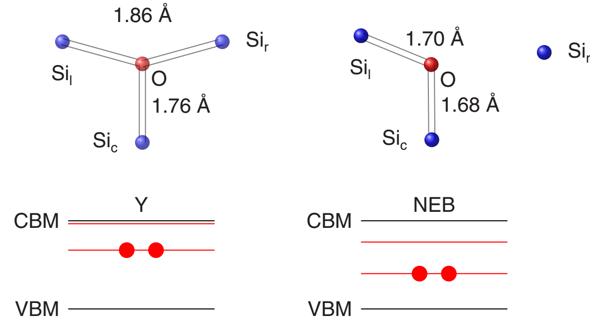

FIG. 3. (Color online) Comparison between atomic structures of the symmetric Y-lid configuration and the NEB transition state, as obtained with the PBE functional. The bottom schemes illustrate the positions of the corresponding highest occupied and lowest unoccupied single-particle states in the band gap, as obtained with the HSE functional.

Using the NEB method with 25 images in which all atoms of the supercell are allowed to relax, we obtain the converged description of the minimum energy path for the O migration process (cf. Sec. II D). Figure 2 shows the energy profile as a function of the angle Θ_O, as calculated with the PBE and HSE functionals. For PBE, we find an energy barrier of 1.91 eV, to be compared with the experimental value of 2.53 eV [13,20]. This result confirms a general trend by which the barrier obtained with semilocal functionals is significantly lower than the experimental value. At variance, the energy barrier with the HSE functional increases to 2.52 eV, bringing the calculated value in much closer agreement with the accepted experimental value of 2.53 eV [13,19,20]. A barrier increase of ∼0.3 eV when using hybrid functionals had been observed in a previous study [25], but in the present case the increase is more substantial and the agreement with experiment improved. However, we defer the reader to Sec. II C for a more detailed discussion on the quantitative comparison with the experimental value. From the energy profiles obtained in Fig. 2 it is furthermore evident that the transition state does not occur at the midpoint of the two bond centers. This finding is in good qualitative agreement with the study of Jiang and Brown based on classical interactions [23], but contrasts with all previous density-functional calculations [14,21,22,24–26]. A detailed comparison between the presently found transition state and the competitive symmetric configuration is given in Sec. II B.

B. NEB transition state versus symmetric Y-lid configuration

In all previous density-functional studies [14,21,22,24–26], the transition state consisted of a symmetrically threefold-coordinated oxygen atom occurring at the midpoint between the initial and final states, denoted Y-lid configuration [14]. In order to obtain this configuration, we perform a structural minimization constrained by symmetry using the same setup as in the NEB calculations. We obtain a Y-lid configuration in which the bonds formed by the threefold-coordinated O atom have bond lengths of 1.86 Å with the Si_l and Si_r atoms and of 1.76 Å with Si_c. The structure is illustrated in Fig. 3, where it is compared with that of the transition structure achieved through the NEB calculations.

The Y-lid configuration is found at 1.99 eV higher energy than the equilibrium structure. Hence, this result further supports the NEB calculations which yield a transition state at 1.91 eV in the same conditions, namely with a 64-atom supercell and the PBE functional. Using the HSE hybrid functional for the PBE structure, we find the Y-lid configuration at 2.57 eV, still slightly higher than the corresponding energy for the NEB transition state (2.52 eV).

It is of interest to analyze the physical reasons by which the Y-lid configuration lies at higher energy than the NEB transition state. Let us first focus on the electronic structure. The main difference in the bonding results from an additional Si–O bond in the Y-lid configuration. This extra bond involves the threefold-coordinated O atom and the Si_r atom, and should be compared with the situation in the NEB transition state where this bond is absent, the O atom being regularly bonded in a twofold-coordinated fashion and the Si_r atom carrying an empty dangling bond. The electronic energy involved in such a bond formation is difficult to evaluate as it depends on the degree of residual strain present in the bonds. Nevertheless, estimates of about 1 eV have been put forward for the electronic energy gain due to the formation of such a bond in structurally relaxed conditions [40,41].

There are two mechanisms by which the formation of an extra bond is compensated in the NEB transition state. The first is of electronic origin. Indeed, the Si_c atom in both the Y-lid configuration and the NEB transition state is undercoordinated and carries a localized doubly occupied doublet. By comparing the electronic structures shown in Fig. 3, one notices that the doublet lies at higher energy in the symmetric Y-lid configuration. The energy variation is 0.15 eV with the PBE functional and increases to 0.3 eV with the HSE functional. We attribute this effect to the fact that the symmetric location of the Si_c–O bond destabilizes the dangling bond with respect to the more natural orientation in the asymmetric NEB structure.

The second factor that contributes to the stabilization of the NEB structure is the structural relaxation. The Y-lid configuration naturally introduces strain around the O atom to ensure reasonable bond lengths with Si_r and Si_l. At variance, the NEB transition state is not subject to such constraints and the Si–O–Si structure can optimally relax. To better assess the role of the relaxation of the surrounding Si atoms, we perform a series of additional NEB calculations in which a varying number of Si atoms are constrained to remain fixed at their ideal bulk positions. We first only allow the three closest Si atoms to move together with the O atom during the diffusion process. Using the PBE functional, we find in this case an energy barrier of $\sim$2 eV which does not differ significantly from the fully unconstrained calculation (1.91 eV, cf. Fig. 2). However, the transition path now shows a symmetric behavior. To recover an asymmetric transition profile, it is necessary that all atoms up to the second nearest neighbor Si atoms be allowed to vary their positions during the transition.

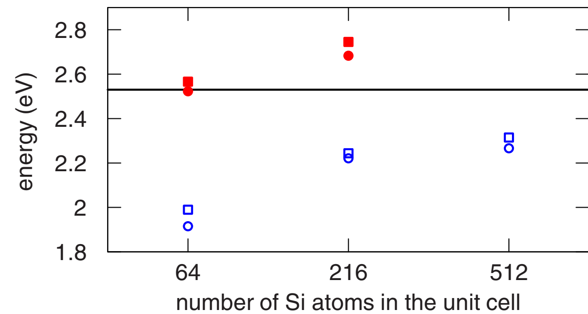

FIG. 4. (Color online) Transition barrier of the NEB transition state (circles) in calculations with unit cells of increasing size, as obtained with PBE (open symbols, blue) and HSE (closed symbols, red) functionals. The energy pertaining to the symmetric Y-lid configuration is also shown (open blue and closed red squares). The horizontal line at 2.53 eV corresponds to the experimental value given in Refs. [13,19,20].

C. Convergence with supercell size

It is important to address the validity of the achieved results against the convergence with supercell size and **k**-point sampling, as it is known that the convergence of defect calculations in silicon might be particularly tedious [42,43]. We adopt the strategy of considering supercells of increasing size, while retaining the sole Γ point in the **k**-point sampling. Based on previous defect calculations in silicon [42], **k**-point samplings other than the Γ point are expected to converge to the same value for supercells of about 216 atoms or larger.

For each adopted supercell, we compare the energy of both the NEB transition state and the Y-lid configuration with respect the equilibrium Si–O–Si configuration. The NEB optimization is computationally too expensive to be carried out on cells larger than 64 atoms. For the NEB structure in the larger supercells, we thus adopt a procedure by which the structural coordinates up to the second shell of Si atoms are taken from the 64-atom supercell and kept fixed while all more distant atoms are allowed to undergo relaxation. This approach is expected to properly account for the electronic energy, while the uncomplete account of the relaxation might lead to a small overestimation of the NEB transition-state energy. However, on the basis of calculations performed for the ground state and the Y-lid configuration, we find an estimate of only 0.06 eV for the deviation by which such an overestimation exceeds the targeted value. Finally, the energies of the three structures in the 216-atom supercell obtained in this way are also evaluated with the HSE functional.

The calculated energies are reported in Fig. 4. We first remark that the NEB configuration is always found to be lower than the corresponding Y-lid configuration. In consideration of the incomplete relaxation of the former configuration, the energy separation is expected to be actually even larger than reported in Fig. 4. Second, we notice that the 64-atom results are not converged with supercell size. Focusing on the PBE results, we remark that the energies obtained undergo significant variations going from a 64-atom to a 216-atom cell. The PBE transition barrier is found to increase to 2.22 eV in the case of a 216-atom supercell. A further increase of the supercell size to 512 atoms, gives a barrier of 2.27 eV, barely different from the result achieved with the 216-atom supercell. Our best estimate for the PBE transition barrier is thus 2.3 eV, with errors expected to be of the order of 0.1 eV. Furthermore, we conclude that the results achieved with 216-atom cells are converged within about 0.1 eV. Thus, we estimate the HSE barrier to be 2.7 ± 0.1 eV on the ground of the 216-atoms supercell calculations. In comparison with the experimental value, our study of the convergence with supercell size leads us to the conclusion that the PBE value (2.3 eV) underestimates the experimental value (2.53 eV, Refs. [13,19,20]) by about 0.2 eV, whereas the HSE functional yields an overestimation by about the same amount. The small size of these deviations indicate a fair agreement between theory and experiment.

D. Convergence with number of images in NEB method

The NEB method enables convergence of the minimum energy path provided a sufficient number of images is used [27]. A small number of images might not only lead to an insufficient resolution near the saddle point [44], but also affect the accuracy of the force projection ("nudging") which depends on successive images [27,45]. The occurrence of two competitive paths might enhance the effect of such inaccuracies when using a low number of images. We therefore investigate the convergence of the energy profile and the

TABLE I. Convergence of the energy barrier E_b and the angle Θ_O at the transition state with number of images N_i used in the nudged elastic band method. $\Delta\Theta_O$ indicates the variation undergone by Θ_O when considering the images closest to the transition-state image and can thus be taken as error for the determination of Θ_O. For $N_i \leqslant 9$, the diffusion path appears nearly symmetric with respect to $\Theta_O = 0$.

N_i	Θ_O	$\Delta\Theta_O$	E_b (eV)
9	-2.5°	$\pm 8^\circ$	2.19
11	2°	$\pm 8^\circ$	1.80
15	8°	$\pm 6^\circ$	1.91
17	22°	$\pm 2^\circ$	1.94
25	26°	$\pm 1^\circ$	1.91

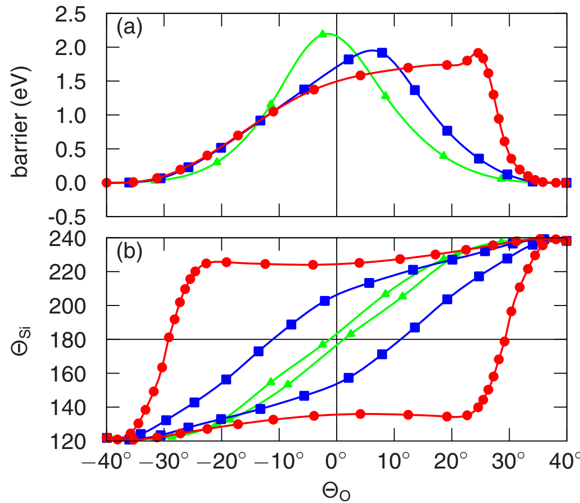

FIG. 5. (Color online) Evolution of (a) the energy and (b) the principal structural parameters Θ_O and Θ_{Si} along the transition path for NEB calculations based on the PBE functional with different numbers of images: $N_i = 9$ (triangles, green), $N_i = 15$ (squares, blue), and $N_i = 25$ (disks, red). In (a), the energy profile for only one of the possible equivalent transitions is shown, whereas the paths of both equivalent transitions are shown in (b).

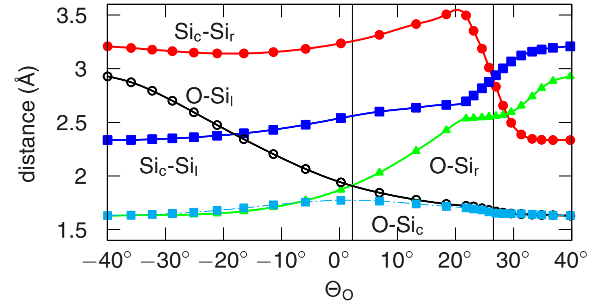

FIG. 6. (Color online) Evolution of distances between relevant atoms during the transition, as obtained with the NEB calculations based on the PBE functional: Si_c–Si_l (filled disks, red), Si_c–Si_r (filled squares, blue), O–Si_l (open disks, black), O–Si_c (filled small squares, cyan), and O–Si_r (filled triangles, green). The vertical line at $\Theta_O \cong 2°$ indicates the position where the O–Si_l and O–Si_r bond lengths are equal. The vertical line at $\Theta_O \cong 26°$ indicates the position where the Si_c–Si_l and Si_c–Si_r distances are equal. The equilibrium PBE Si–Si distance in bulk silicon is 2.36 Å.

main structural parameters as the number of intermediate images (N_i) in the NEB calculations is increased. We perform these calculations with 64-atom supercells and with a **k**-point sampling at the Γ point, with the same setup as in Sec. II A.

The results of this analysis are given in Table I and Fig. 5. We observe that the calculated energy barriers remain constant within a few tenths of an electron volt (1.80–2.19 eV), whereas the features of the transition path undergo significant changes with increasing N_i. For N_i up to 9, the transition path is essentially symmetric, but, as N_i increases further, the saddle point moves out of the mid-point of the two bond centers and progressively occurs at larger Θ_O. Finally, it reaches a converged value at $\Theta_O \cong 26°$. By monitoring both Θ_O and Θ_{Si} through the transition path in Fig. 5(b), one understands how the asymmetric energy profile for the O transition takes its origin from a complex motion which involves the nearby Si atoms. The present analysis also provides a rationale for understanding the differences between our result and previous NEB calculations with a smaller number of images which yielded a symmetric transition path [26].

III. ATOMISTIC MECHANISM

In the present section, we analyze the minimum energy path obtained in Sec. II A through the NEB calculations from the viewpoint of the evolution of bond distances, maximally localized Wannier functions, and single-particle electronic states.

A. Structural evolution

First, we analyze the diffusion path through the evolution of the distances between the relevant atoms (cf. Fig. 6). During the transition, the distance between Si_c and the interstitial O atom undergoes only minor variations from 1.63 Å in the equilibrium position to 1.77 Å at $\Theta_O \cong 0°$. Until $\Theta_O \cong -6°$, the interstitial O is twofold coordinated, with the O–Si_c and O–Si_r distances remaining approximately equal. As Si_l approaches, a threefold coordinated O atom is formed at $\Theta_O \cong 2°$, with the O–Si_c, O–Si_l, and O–Si_r bond lengths being equal to 1.77, 1.91, and 1.91 Å, respectively. Then, the roles of Si_l and Si_r exchange. As the O–Si_r distance increases, the O–Si_l distance progressively decreases to reach the value pertaining to a twofold-coordinated O atom. From $\Theta_O \cong 22°$ and until $\Theta_O \cong 30°$, the O–Si_r distance reaches a plateau at ∼2.6 Å. In the final part of the diffusion process, the O–Si_r increases again at a faster rate and reaches the final value of 2.93 Å in the new equilibrium position.

The diffusion process can also be followed by monitoring the Si–Si distances. The Si_c–Si_l and Si_c–Si_r distances undergo only gradual changes until $\Theta_O \cong 22°$. The Si_c–Si_l distance is found to increase continuously from 2.33 to 2.69 Å, whereas the Si_c–Si_r distance first decreases from 3.21 to 3.14 Å at $\Theta_O \cong -15°$ and then increases to 3.50 Å at $\Theta_O \cong 22°$. From $\Theta_O \cong 22°$ and until $\Theta_O \cong 30°$, the roles of Si_l and Si_r exchange. The Si_c–Si_r distance decreases strongly to 2.44 Å, whereas the Si_c–Si_l distance increases strongly to 3.10 Å. At $\Theta_O \cong 26°$, the Si_c–Si_l and Si_c–Si_r distances are equal.

This analysis shows that the exchange between O-Si distances and Si–Si distances occurs at different Θ_O. This indicates that the transition cannot be understood exclusively in terms of the formation and breaking of Si–O bonds. More surprisingly, the value of Θ_O for which the transition barrier is obtained coincides with that of the exchange of the Si–Si distances.

B. Description in terms of Wannier centers

A purely structural analysis of the diffusion path does not account explicitly for the evolution of the electronic structure during the transition. Deeper insight can be achieved by focusing on the centers of maximally localized Wannier functions which carry information about the electronic structure in a compact form [46]. We thus calculate the positions of the

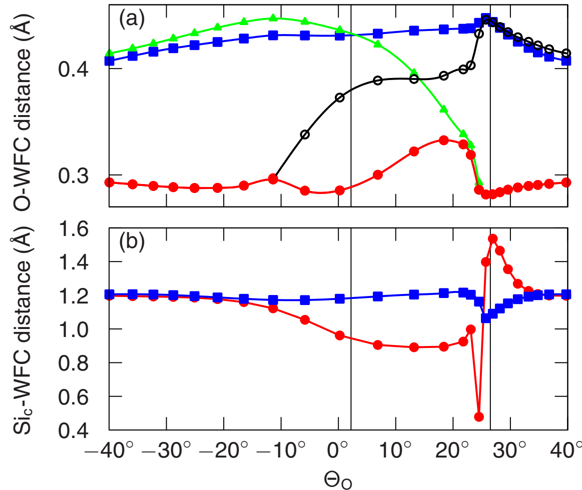

FIG. 7. (Color online) Evolution of the distances of the relevant Wannier-function centers with respect to (a) the O atom and (b) the central Si atom (Si$_c$), as obtained with the NEB calculations based on the PBE functional. In (a), one of the WFCs corresponds to a lone pair throughout the transition (closed disks, red), while another WFC remains associated to the Si$_c$–O bond (squares, blue). One of the remaining WFCs (triangles, green) first represents the bond to Si$_r$, but then evolves to a lone pair. The fourth WFC (open disks, black) undergoes the opposite evolution from representing a lone pair to a bond with Si$_l$. In (b), one of the WFCs (disks, red) represents the moving electrons in the process (cf. Fig. 8). The two WFCs (squares, blue) representing the backbonds between Si$_c$ and the bulk Si atoms are also shown. The fourth WFC corresponds to the Si$_c$–O bond, does not undergo any interesting variation [cf. curve with squares in (a)], and is not shown. The vertical lines are defined in the caption of Fig. 6.

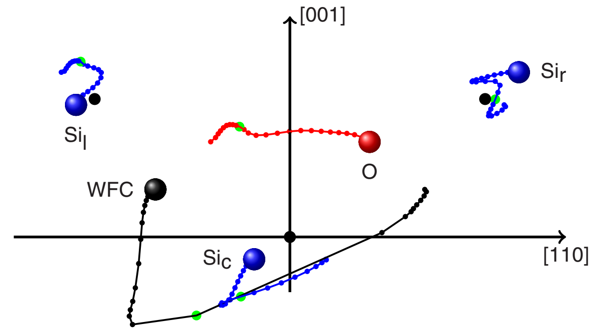

FIG. 8. (Color online) Transition path of the atoms and of the Wannier function center pertaining to the Si–Si bond during the O diffusion step. The large balls represent the initial positions. The small black dots correspond to the ideal Si positions in the unperturbed bulk. The beads on the path sequentially correspond to the images of the nudged-elastic-band method. On each path, the large green bead corresponds to the saddle point of the transition at $\Theta_O \cong 26°$.

Wannier function centers (WFCs) and study their evolution through the transition.

In an unperturbed Si crystal, each Si–Si bond shows one doubly occupied WFC in the middle of the bond. In SiO_2, in which each O atom forms two Si–O bonds, four doubly occupied WFCs are located around each O atom. Two of those are responsible for the bond formation with the neighboring Si atoms, while the other two correspond to the lone pairs of the O atom.

Figure 7(a) shows the distances between the O atom and its neighboring WFCs. When the O atom is twofold coordinated there are two WFCs representing lone pairs. At $\Theta_O \cong -11°$, the distance between one of these WFCs and the O atom starts increasing as the bond between O and Si$_l$ gradually forms. This can be interpreted as a mark leading to the formation of a threefold-coordinated O atom. Indeed, the WFC corresponding to the Si$_r$–O bond concurrently reduces its distance to the O atom. At $\Theta_O \cong 13°$, a crossing is observed between the distances of these two WFCs. This configuration occurs as the WFCs exchange their role and can be taken as the signature of a threefold coordinated O atom within the Wannier function description. We note that this signature occurs at a higher value of Θ_O than inferred from the structural point of view in Fig. 6 ($\Theta_O \cong 13°$ vs $\Theta_O \cong 2°$). When $\Theta_O > 25°$, there are again two WFCs at distances typical of the lone pairs and the O atom recovers a twofold coordination.

There are four WFCs evolving around the central Si atom (Si$_c$). One of these corresponds to the Si$_c$–O bond and is constantly found in the vicinity of the O atom [blue squares in Fig. 7(a)], as this bond is preserved during the transition (Fig. 6). The distances at which the other three WFCs evolve are shown in Fig. 7(b). Two of these WFCs represent the backbonds that keep Si$_c$ attached to the bulk and undergo only minor variations during the transition.

The most interesting evolution concerns the WFC associated with the bond between Si$_c$ and Si$_l$ which switches to the bond between Si$_c$ and Si$_r$ as the transition proceeds. In the initial and final equilibrium positions, this WFC represents two electrons in a normal Si–Si bond. During the transition, it undergoes large distance variations for small variations of Θ_O, from a minimal distance of 0.48 Å at $\Theta_O \cong 24.5°$ to a maximal distance of 1.53 Å at $\Theta_O \cong 26.9°$. These important fluctuations occur in correspondence of the Si–Si bond switching transition and are associated with large Wannier-function spreads. For instance, the Wannier function spread at $\Theta_O \cong 24.5°$ attains a value which is more than three times larger than that of a regular Si–Si bond. The transition path of this WFC is displayed in Fig. 8 together with those of the nearby O and Si atoms. One observes that the WFC of the Si$_c$–Si$_l$ bond is gradually pushed away as the O atom approaches and finally flips to the other side as the Si$_c$–Si$_r$ bond is formed.

C. Electronic-structure evolution

In this section, we complement the discussion about the electronic-structure evolution by addressing the single-particle energy levels as obtained with the HSE functional. The highest occupied and the lowest unoccupied energy levels are shown in Fig. 9 as the O atoms moves across the saddle point. At the beginning of the diffusion process, the highest occupied state essentially coincides with the valence band edge of the unperturbed crystal. The character of this state corresponds to that of bonding Si–Si orbitals. The Si–O bonds are found at lower energies.

As the O moves across the saddle point, the highest occupied state rises up to 0.48 eV in the band gap. As it

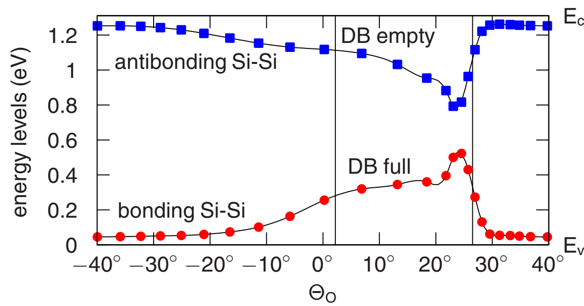

FIG. 9. (Color online) Highest occupied and lowest unoccupied single-particle energy levels as obtained with the HSE functional during the transition. The horizontal lines indicate the valence band edge (E_v) and the conduction band edge (E_c), respectively. The occupied dangling bond (DB full) is localized on Si_c, while the unoccupied dangling bond (DB empty) is localized on Si_r. The vertical lines are defined in the caption of Fig. 6.

separates from the valence band, the associated orbital localizes and becomes a doubly occupied dangling bond located at Si_c, in accord with the Wannier function analysis in Fig. 8. After the crossing involving the Si_c–Si_l and Si_c–Si_r distances at $\Theta_O \cong 26^\circ$, the dangling bond recovers a Si–Si bonding character and its single-particle energy level returns to the valence band edge.

Further insight into the electronic behavior can be acquired by inspection of the single-particle orbitals. Figure 10 shows the orbitals of the highest occupied and lowest unoccupied states for four selected atomic configurations occurring during the transition. When $\Theta_O \cong -40^\circ$, the atoms occupy the equilibrium configuration [Fig. 10(a)]. In this configuration, the highest occupied state is delocalized and is not visualized in our description. At variance, the lowest unoccupied state localizes on the two Si neighbors of the O atom and shows an antibonding character. At $\Theta_O \cong 0^\circ$, the O atom has become threefold coordinated [Fig. 10(b)]. In this configuration, the charge density of the highest occupied state corresponding to the Si–Si bond has moved towards Si_c, in accord with the position of the associated WFC (cf. Fig. 8). The lowest unoccupied state is also localized, but appears distributed over all four atoms. At $\Theta_O \cong 23^\circ$, the O atom has already exchanged its neighbors while the Si_c–Si_r is still to be formed [Fig. 10(c)]. This configuration corresponds to the image with the second-highest energy in Fig. 2 and is thus very close to the saddle point. One notices that the charge density of the highest occupied state around Si_c has localized further, consistent with the formation of a doubly occupied dangling bond. The weight of the lowest unoccupied state is mostly localized around Si_r and can be interpreted as an empty dangling bond. Figure 10(d) corresponds to the first NEB image after the energy maximum ($\Theta_O \cong 26^\circ$). The charge density of the highest occupied state has moved towards the midpoint between Si_c and Si_r, indicating the formation of the new bond. The lowest unoccupied state also localizes around Si_c and Si_r, as expected for the antibonding state associated with the Si_c–Si_r bond.

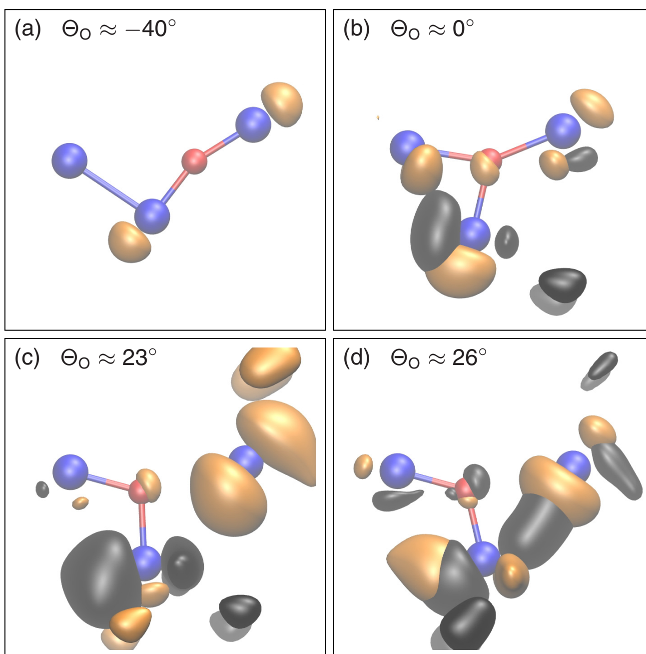

FIG. 10. (Color online) Highest occupied (dark shade, black) and lowest unoccupied (light shade, orange) single-particle orbitals at selected Θ_O during the transition. The red and blue balls represents the O atom and its neighboring Si atoms, respectively.

IV. CONCLUSION

We studied the elementary diffusion step of a single interstitial O atom in bulk silicon when hopping from one bond-center site to an adjacent one in a (110) plane within an approach based on semilocal and hybrid density functionals. First, we obtained a detailed description of the minimum energy path using the nudged elastic band method. Upon careful convergence studies with the size of the supercell, we obtained for the transition barrier best estimates of 2.3 and 2.7 eV in the generalized gradient approximation (PBE) and in the hybrid functional scheme (HSE), respectively. Both estimates show a fair agreement with the commonly accepted experimental value of 2.53 eV [13,19,20]. Thus, the identified elemental diffusion step accounts sufficiently well for the long-range diffusion without the necessity of invoking peculiar mechanisms [21] or multiple paths [24].

Our study gives a saddle point that does not occur at the midpoint between the bond-center sites. We find that the achieved saddle point is lower in energy by only about 0.1 eV when compared with the symmetric Y-lid configuration consisting of a threefold coordinated O atom, which was often identified as the transition state in previous studies. In particular, we showed that the pattern of displacements extending up to the shell of second nearest neighbor Si atoms lies at the origin of the asymmetric minimum energy path found in our nudged elastic band calculations. The present result qualitatively reconciles the density-functional result with that obtained previously with classical interaction potentials [23]. All previous density functional studies [14,21–26] have been unable to reach such a description, most likely because of the difficulty of properly describing the transition path in a computationally demanding scheme. This difficulty is

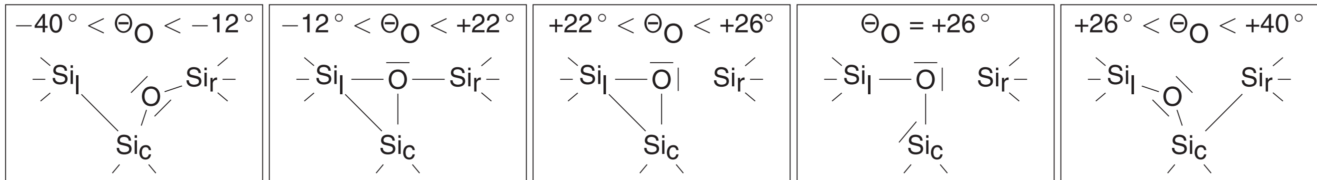

FIG. 11. Schematic evolution of the atomic positions and the electronic states as the O atoms moves across the transition. Each stick represents two electrons.

overcome in the present study through the use of a sufficiently large number of images in the nudged-elastic-band method.

We then analyzed the underlying atomistic mechanism studying the evolution of the atomic and electronic structure across the transition. This analysis revealed a mechanism which is schematically represented in Fig. 11. Up to $\Theta_O \cong -12^\circ$, the O atom is twofold coordinated and all Si atoms are fourfold coordinated. Then, for $-12 < \Theta_O < 12$, the O atom moves and forms an extra bond with Si_l. The oxygen atom becomes thus threefold coordinated while Si_l is momentarily fivefold coordinated. The other two Si atoms remain regularly coordinated. Between $\Theta_O \cong 22^\circ$ and $\Theta_O \cong 26^\circ$, the O atom becomes twofold coordinated leaving an unoccupied dangling bond on Si_r. Si_l is still fivefold coordinated but the charge density in the Si_c–Si_l bond progressively displaces towards Si_c. At $\Theta_O \cong 26^\circ$, the bond between Si_l and Si_c breaks and the electrons originating from this bond condensate in a doubly occupied dangling bond on Si_c. This corresponds to the saddle point in the transition energy profile. The transition completes by the dangling bond flipping around Si_c and building up the charge density in the Si_c–Si_r bond.

This analysis reveals a peculiar mechanism by which the diffusion process can be separated in two distinct parts. One part concerns the exchange of the Si atoms within the first-neighbor shell of the diffusing O atom. The other part corresponds to the flipping of the Si–Si bond from its initial to its final position. The occurence of these two parts allows us to rationalize the underlying structure observed in the calculated transition energy profile (cf. Fig. 2). The wide barrier which dominates the transition energy profile mainly arises from the formation of the threefold coordinated O center, whereas the narrow peak occurring at $\Theta_O \cong 26^\circ$ corresponds to the formation of occupied and unoccupied dangling bonds upon the flipping of the Si–Si bond.

ACKNOWLEDGMENTS

Financial support from the Swiss National Science Foundation (Grants No. 200020-119733/1, No. 206021-128743, and No. 200020-134600/1) is acknowledged. We used computational resources of CSCS and CSEA.

[1] B. E. Deal and A. S. Grove, J. Appl. Phys. **36**, 3770 (1965).
[2] E. P. Gusev, H. C. Lu, T. Gustafsson, and E. Garfunkel, Phys. Rev. B **52**, 1759 (1995).
[3] A. Pasquarello, M. S. Hybertsen, and R. Car, Nature (London) **396**, 58 (1998).
[4] *Fundamental Aspects of Silicon Oxidation*, edited by Y. J. Chabel (Springer, Berlin, 2001).
[5] A. M. Stoneham, M. A. Szymanski, and A. L. Shluger, Phys. Rev. B **63**, 241304 (2001).
[6] A. Bongiorno and A. Pasquarello, Phys. Rev. Lett. **88**, 125901 (2002).
[7] A. Bongiorno and A. Pasquarello, Phys. Rev. B **70**, 195312 (2004).
[8] A. Bongiorno and A. Pasquarello, Phys. Rev. Lett. **93**, 086102 (2004).
[9] A. Alkauskas, P. Broqvist, and A. Pasquarello, Phys. Rev. B **78**, 161305(R) (2008).
[10] A. Pasquarello, M. S. Hybertsen, and R. Car, in *Fundamental Aspects of Silicon Oxidation*, edited by Y. J. Chabal (Springer, Berlin, 2001), p. 107.
[11] *Oxygen in Silicon*, edited by F. Shimura, Semiconductors and Semimetals Vol. 42 (Academic, Orlando, 1994).
[12] *Early Stages of Oxygen Precipitation in Silicon*, edited by R. Jones, NATO Advanced Science Institution, Series 3: High Technology, Vol. 17 (Kluwer, Dordrecht, 1996).
[13] R. C. Newman, J. Phys.: Condens. Matter **12**, R335 (2000).
[14] J. Coutinho, R. Jones, P. R. Briddon, and S. Öberg, Phys. Rev. B **62**, 10824 (2000).
[15] H. J. Hrostowski and R. H. Kaiser, Phys. Rev. **107**, 966 (1957).
[16] W. L. Bond and W. Kaiser, J. Phys. Chem. Solids **16**, 44 (1960).
[17] J. W. Corbett, R. S. McDonald, and G. D. Watkins, J. Phys. Chem. Solids **25**, 873 (1964).
[18] P. D. Southgate, Proc. Phys. Soc. London **76**, 385 (1960).
[19] G. D. Watkins, in *Early Stages of Oxygen Precipitation in Silicon*, edited by R. Jones (Kluwer, Dordrecht, 1996), p. 1.
[20] J. C. Mikkelsen, Mater. Res. Soc. Symp. Proc. **59**, 19 (1985).
[21] M. Needels, J. Joannopoulos, Y. Bar-Yam, S. Pantelides, and R. H. Wolfe, Mater. Res. Soc. Symp. Proc. **209**, 103 (1991).
[22] A. Oshiyama and M. Saito, in *Defect Control in Semiconductors*, edited by K. Sumino (North-Holland, Amsterdam, 1990).
[23] Z. Jiang and R. A. Brown, Phys. Rev. Lett. **74**, 2046 (1995).
[24] M. Ramamoorthy and S. T. Pantelides, Phys. Rev. Lett. **76**, 267 (1996).
[25] P. Deák, B. Aradi, T. Frauenheim, and A. Gali, Mater. Sci. Eng. B **154–155**, 187 (2008).
[26] S. K. Estreicher, D. J. Backlund, C. Carbogno, and M. Scheffler, Angew. Chem. Int. Ed. **50**, 10221 (2011).
[27] H. Jónsson, G. Mills, and K. W. Jacobsen, in *Classical and Quantum Dynamics in Condensed Phase Systems*, edited by B. J. Berne, G. Ciccotti, and D. F. Coker (World Scientific, Singapore, 1998), p. 385.

[28] J. P. Perdew, K. Burke, and M. Ernzerhof, Phys. Rev. Lett. **77**, 3865 (1996).
[29] J. Heyd, G. E. Scuseria, and M. Ernzerhof, J. Chem. Phys. **118**, 8207 (2003); **124**, 219906 (2006).
[30] N. Troullier and J. L. Martins, Phys. Rev. B **43**, 1993 (1991).
[31] *CRC Handbook of Chemistry and Physics*, 69th ed., edited by R. C. Weast (CRC Press, Boca Raton, FL, 1988).
[32] M. A. Hopcroft, W. D. Nix, and T. W. Kenny, J. Microelectromech. S. **19**, 229 (2010).
[33] A. F. Wright and M. S. Lehmann, J. Solid State Chem. **36**, 371 (1981).
[34] R. Tarumi, K. Nakamura, H. Ogi, and M. Hirao, J. Appl. Phys. **102**, 113508 (2007).
[35] L. Levien, C. T. Prewitt, and D. Weidner, Am. Miner. **65**, 920 (1980).
[36] P. Broqvist, A. Alkauskas, and A. Pasquarello, Phys. Rev. B **80**, 085114 (2009).
[37] P. Giannozzi, S. Baroni, N. Bonini, M. Calandra, R. Car, C. Cavazzoni, D. Ceresoli, G. L. Chiarotti, M. Cococcioni, I. Dabo *et al.*, J. Phys.: Condens. Matter **21**, 395502 (2009).
[38] H.-P. Komsa, P. Broqvist, and A. Pasquarello, Phys. Rev. B **81**, 205118 (2010).
[39] J. Paier, M. Marsman, K. Hummer, G. Kresse, I. C. Gerber, and J. G. Ángyán, J. Chem. Phys. **124**, 154709 (2006); **125**, 249901 (2006).
[40] J. Godet, F. Giustino, and A. Pasquarello, Phys. Rev. Lett. **99**, 126102 (2007).
[41] J. F. Binder, P. Broqvist, and A. Pasquarello, Physica B **407**, 2939 (2012).
[42] M. J. Puska, S. Pöykkö, M. Pesola, and R. M. Nieminen, Phys. Rev. B **58**, 1318 (1998).
[43] M. Pesola, J. von Boehm, and R. M. Nieminen, Phys. Rev. Lett. **82**, 4022 (1999).
[44] G. Henkelman, B. P. Uberuaga, and H. Jónsson, J. Chem. Phys. **113**, 9901 (2000).
[45] G. Henkelman and H. Jónsson, J. Chem. Phys. **113**, 9978 (2000).
[46] N. Marzari and D. Vanderbilt, Phys. Rev. B **56**, 12847 (1997).